

Unraveling how winds and surface heat fluxes control the Atlantic Ocean's meridional heat transport

Dhruv Bhagtani^{1,2*}, Andrew McC. Hogg^{1,2,3},
Ryan M. Holmes⁴, and Navid C. Constantinou^{3,5}

¹Research School of Earth Sciences, Australian National University, Canberra, ACT, Australia

²ARC Center of Excellence for Climate Extremes, Australia

³ARC Center of Excellence for the Weather of the 21st Century, Australia

⁴Australian Bureau of Meteorology, Sydney, NSW, Australia

⁵School of Geography, Earth and Atmospheric Sciences, University of Melbourne, Parkville, VIC, Australia

Key Points:

- We quantify the individual impact of winds and surface heat fluxes on Atlantic Ocean's heat transport using ocean model simulations
- The circulation response to forcing dominates heat transport initially, while temperature structure changes feed back after several decades
- Heat transport at warm temperatures (the gyre) is sensitive to wind forcing while at cold temperatures it is sensitive to buoyancy forcing

Abstract

The North Atlantic Ocean circulation, fueled by winds and surface buoyancy fluxes, carries 1.25 PettaWatts of heat poleward in the subtropics, and helps in regulating global weather and climate patterns. Here, we assess the impacts of changes in winds and surface heat fluxes on the Atlantic Ocean circulation and heat transport using ocean simulations. We decompose the circulation and heat transport into warm and cold cells (resembling a subtropical gyre and the dense overturning circulation respectively), and a mixed cell capturing waters transitioning between warm and cold regions. Warm and mixed cells transport more heat poleward as wind stress increases; however, these anomalies are compensated by reductions in the cold cell's heat transport. Warm and cold cells transport more heat poleward when we increase meridional heat flux gradients. Our findings underscore the distinct roles of winds and surface heat fluxes in controlling the Atlantic Ocean's meridional heat transport.

Plain Language Summary

The Earth gains heat from the sun in the tropics and loses heat near the poles. To maintain a balance, the large-scale circulation in the ocean and the atmosphere must carry heat from the tropics to the poles. Here, we focus on the Atlantic ocean circulation, which is jointly fueled by winds and surface heat and freshwater inputs, and try to understand how this movement of heat poleward is affected by these surface forcings. To do so, we use global ocean model simulations in which we change either winds or surface heat fluxes across the globe, and analyze how the poleward heat transport changes in each set of experiments. We further split the ocean circulation into three components: (*i*) currents flowing near the ocean's surface, (*ii*) currents in the deep ocean, and (*iii*) mixed waters that have the ability to traverse both near-surface and deep ocean currents. We then identify which bit of the circulation carries heat poleward and how they are affected by the forcings. We find that the near-surface ocean currents and their associated poleward heat transport are quick to

*142 Mills Road, Acton, 2601, ACT, Australia

Corresponding author: Dhruv Bhagtani, dhruv.bhagtani@anu.edu.au

respond to changes in winds, while the deep ocean currents react relatively slowly to changes in surface heat inputs.

1 Introduction

The oceanic and atmospheric circulation together advect around 5.5 PW (1 PW \equiv 10^{15} W) of heat poleward to regulate global weather and climate patterns (Masuda, 1988). Modeling studies (Msadek et al., 2013; Stepanov et al., 2016; Liu et al., 2022) and hydrographic surveys (Johns et al., 2011; Trenberth et al., 2019; Frajka-Williams et al., 2019) estimate that the large-scale North Atlantic Ocean circulation, driven by a combination of winds and surface buoyancy fluxes, transfers ≈ 1.25 PW heat poleward in the subtropics, which is about three-quarters of the total oceanic heat transport at these latitudes. Future changes in the Atlantic Ocean's circulation and heat transport are expected due to climate change-induced variability in surface forcing (Mecking & Drijfhout, 2023). Such variations include the intensification of westerlies (Shaw & Miyawaki, 2024) and polar amplification (Rantanen et al., 2022), yet the relative importance of winds and surface heat fluxes in driving the Atlantic Ocean's meridional heat transport (MHT) is not fully understood.

The Atlantic Ocean circulation is dominated by two distinct (albeit interconnected) mechanisms. First, convection in the subpolar North Atlantic produces dense water that contributes to driving the deep arm (between 1000 m–3000 m) of the Atlantic Meridional Overturning Circulation (AMOC) (Cessi, 2019). The AMOC transfers heat northward in both hemispheres (Bryan, 1991; Frajka-Williams et al., 2019). Additionally, a shallow (upper ~ 1000 m) subtropical gyre, traditionally believed to be driven by wind stress (Sverdrup, 1947), carries warm waters poleward via the Gulf Stream, with a relatively colder equatorward flow. Since the AMOC and subtropical gyre are thought to be primarily influenced by different physical mechanisms, isolating the two circulatory features can reveal dynamical links between surface forcing (e.g., winds and surface heat fluxes) that drives circulation and resultant heat transport.

Several techniques have been used to isolate the AMOC and the subtropical gyre. One method based on Eulerian averaging (Hall & Bryden, 1982; Bryan, 1982) equates the AMOC heat transport at any given latitude to the vertical integral of the product of a zonally-averaged velocity and a zonally-averaged temperature, with the residual equal to the gyre's MHT. This Eulerian-based decomposition designates the vertical component as the primary driver of the Atlantic MHT due to a larger temperature difference between its warmer northward and colder southward branches (Wunsch & Roemmich, 1985; Bryden & Imawaki, 2001). However, flow across isopycnals is weak compared to flow along isopycnals (Abernathy et al., 2022), therefore, a decomposition in depth space may not realistically separate the subtropical gyre and the AMOC.

Potential density or temperature can be used to partition the ocean circulation. Boccaletti et al. (2005) and Greatbatch and Zhai (2007) separate the circulation in temperature space and find similar magnitudes of MHT by the resulting subtropical gyre and the AMOC. Talley (2003) used density to divide the ocean into shallow, intermediate, and deep waters and found similar northward heat contributions of the shallow and deep water masses (corresponding to a gyre and an inter-hemispheric overturning, respectively), in line with Boccaletti et al. (2005) and Greatbatch and Zhai (2007). In contrast, using output from numerical models alongside RAPID array observations, Xu et al. (2016) found that the subtropical gyre (isopycnal flow above a potential density referenced to 2000 dbar of 34.75 kg m^{-3}) carries a small net southward heat flux in density space. Since the Gulf Stream is warmer than the corresponding return flow, it is unusual that the subtropical gyre defined by Xu et al. (2016) carries heat southward and suggests a limitation of defining the gyre in density space. Jones et al. (2024) further speculate that this southward MHT may be because the Gulf Stream does not necessarily follow isopycnal contours. Given this issue with partitioning in density space, we instead decompose the circulation in temperature space to

understand the role of warm and cold circulations (resembling the subtropical gyre and the AMOC respectively) in carrying heat poleward.

The gyre and the AMOC have recently been shown to be coupled (Berglund et al., 2022), therefore, a complete delineation between the two features may not be correct (Johns et al., 2023). This coupling is acknowledged in the decomposition by Ferrari and Ferreira (2011), who extend the latitude–temperature framework of Boccaletti et al. (2005) to include a mixed circulation that captures water masses transiting between warm and cold temperatures. In this paper, we decompose the Atlantic Ocean circulation in latitude–temperature space into a warm, cold, and mixed cell following Ferrari and Ferreira (2011) (section 2). We analyze a series of flux-forced simulations (described in section 2) in which we completely separate the effects of wind stress and surface buoyancy forcing from each other. These simulations differ from Ferrari and Ferreira (2011) in that they are more suitable to answer our main research question: how does each surface forcing *independently* contribute to the Atlantic Ocean’s MHT? We present our findings in section 3 and discuss their implications in section 4.

2 Models and methods

2.1 Model setup

We run a series of ocean simulations using the Modular Ocean Model 5 (Griffies, 2012) (at 0.25° horizontal resolution with 50 unevenly spaced vertical levels) by applying climatological surface boundary fluxes of heat, freshwater, and momentum at a 3-hourly frequency. We name these simulations as “flux-forced simulations” on account of prescribed surface forcing. The boundary fluxes are computed from the last 20 years (orange bar in Fig. 1a) of a 670-year-long equilibrated ACCESS-OM2 ocean–sea ice model simulation (Kiss et al., 2020). The ACCESS-OM2 model is also run at a 0.25° horizontal resolution using repeat year forcing based on the JRA55-do atmospheric reanalysis dataset (Tsujino et al., 2018) and initialized from the World Ocean Atlas 2013 dataset (Locarnini et al., 2013; Zweng et al., 2013). The effect of winds and surface buoyancy fluxes on the ocean is usually computed from bulk formulae (e.g., as done in ACCESS-OM2) and relies on the model’s sea surface temperature and atmospheric variables. By prescribing surface fluxes in our flux-forced simulations, we are able to modify each forcing independent of the other, allowing us to ascertain their relative contributions to the Atlantic Ocean’s MHT. The only remaining buoyancy contribution occurs from frazil ice formation that occurs throughout the water column, hence we are physically motivated to model frazil dynamically in our flux-forced experiments instead of applying a surface flux to simulate its behavior.

The flux-forced control simulation is branched off from the 670-year-long ACCESS-OM2 simulation (black dashed line in Fig. 1a) and allowed to stabilize for 100 years, after which we branch off a series of flux-forced experiments with perturbations restricted to the North Atlantic basin. We categorize these simulations into two types: (*i*) multiplicative variations in wind stress, and (*ii*) additive variations in surface meridional heat flux gradients. Since wind stress curl exerts a significant control on near-surface circulation, we multiply the North Atlantic Ocean’s wind stress by a constant factor (Fig. 1b), which changes the curl by the same proportion. We apply an additive surface meridional heat flux (anomaly map shown in Fig. 1c) with equal and opposite signed anomalies in the subtropics and subpolar regions (smoothly connected using a hyperbolic tangent function). This choice of perturbation is not only expected to change the Atlantic Ocean’s total MHT, but also the heat carried by each cell. The naming of surface heat flux experiments is based on the anomalous surface meridional heat flux contrast applied. For example, the -20 W m^{-2} experiment is constructed by cooling subtropics and warming high latitudes by 10 W m^{-2} (Fig. 1c). Each perturbation experiment is run for 100 years to allow advective responses in both the surface and the deep circulations to variations in surface forcing; the first 10 and last 50 years of each experiment are analyzed.

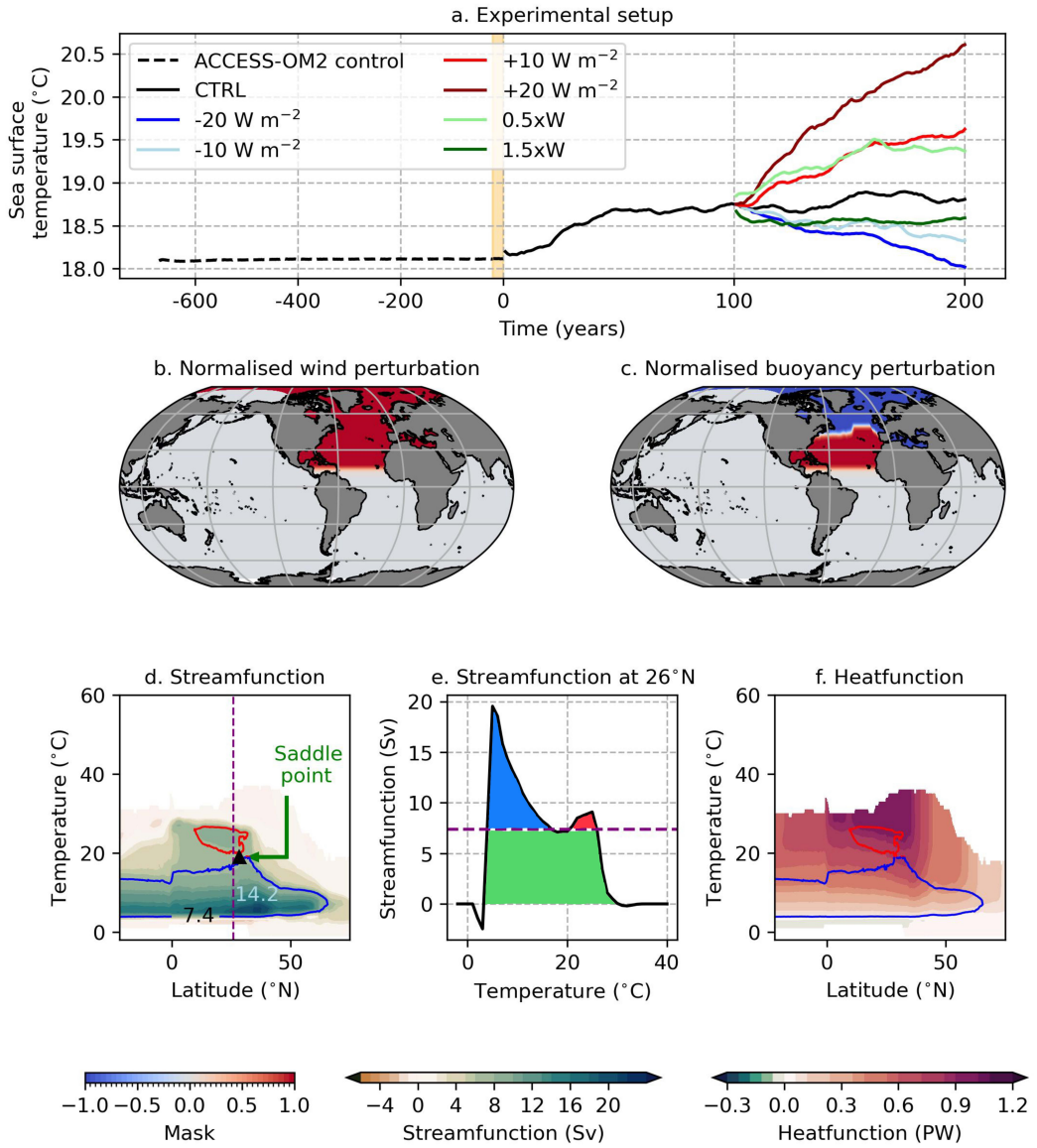


Figure 1. (a). Time series of the mean sea surface temperature for all experiments illustrating the model spinup. (b). Normalized map for zonal and meridional surface wind stress perturbations. The perturbed winds stress is equal to the product of the control's wind stress, the normalized anomaly map, and the desired multiplicative factor. We apply the control's surface wind stress for regions outside the North Atlantic. (c). Normalized map for surface heat flux perturbations. (d). Streamfunction in latitude–temperature space calculated from years 100 – 110 of the CTRL simulation highlighting the strength of the mixed (black text), warm (red text), and cold (blue text) cell. Vertical dashed line denotes 26°N. The black solid triangle marks the saddle point temperature θ_{saddle} . (e). Streamfunction for the 26°N transect marking warm (red), cold (blue), and mixed (green) cells. The horizontal purple line denotes the upper bound of the mixed circulation strength (= 7.4 Sv). (f). Heatfunction in latitude–temperature space obtained by cumulatively integrating the streamfunction in panel (d).

2.2 Definition of warm, cold, and mixed cells in latitude–temperature space

The streamfunction Ψ in latitude–temperature space is defined as (see e.g., Ferrari and Ferreira (2011); Holmes et al. (2019)):

$$\Psi(\phi, \theta, t) \stackrel{\text{def}}{=} R \int_{\lambda_w}^{\lambda_e} \int_{-D}^{\eta} v(\lambda, \phi, z, t) \mathcal{H}(\theta - \theta_c(\lambda, \phi, z, t)) \cos \phi dz d\lambda, \quad (1)$$

where R is the Earth’s radius, λ is longitude, ϕ is latitude, v is meridional velocity, λ_w and λ_e are the western and eastern extents of the Atlantic basin, D is ocean depth, η is sea level, \mathcal{H} is the Heaviside function, and θ_c is conservative temperature (McDougall & Barker, 2011). We compute the streamfunction for $\theta \in [-2, 60]^\circ\text{C}$ and with a 1°C interval; recomputing (1) with 0.5°C or 2°C intervals gave similar results.

The streamfunction (1) for the flux-forced control simulation is shown in Fig. 1d. We divide the clockwise circulation (green contours in Fig. 1) into warm (Ψ_{warm}), cold (Ψ_{cold}), and mixed (Ψ_{mixed}) cells following Ferrari and Ferreira (2011) (also shown for 26°N in Fig. 1e). The warm cell (enclosed by the red contour in Fig. 1d) resembles the subtropical gyre. Similarly, the cold cell (bounded by the blue contour in Fig. 1d) resembles the AMOC. A significant proportion of the clockwise circulation transits around and between the warm and cold cells and is captured by the mixed circulation. The strength of the mixed circulation ($= 7.4 \text{ Sv}$; black text in Fig. 1d) is quantified as the closed streamfunction contour with the smallest value of Ψ that completely isolates the warm and cold cells. This streamfunction contour separates the warm and cold cells at the saddle point (denoted by temperature θ_{saddle} and latitude ϕ_{saddle} in Fig. 1d). After locating the saddle point, we compute the strength of the warm and cold circulations by subtracting the mixed circulation for regions with $\Psi > \Psi_{\text{mixed}}$ (see Fig. 1e) from the streamfunction Ψ . Specifically,

$$\Psi_{\text{warm}} \stackrel{\text{def}}{=} \begin{cases} \Psi - \Psi_{\text{mixed}} & \text{if } \Psi > \Psi_{\text{mixed}} \text{ and } \theta \geq \theta_{\text{saddle}}, \\ 0 & \text{otherwise,} \end{cases} \quad (2)$$

$$\Psi_{\text{cold}} \stackrel{\text{def}}{=} \begin{cases} \Psi - \Psi_{\text{mixed}} & \text{if } \Psi > \Psi_{\text{mixed}} \text{ and } \theta < \theta_{\text{saddle}}, \\ 0 & \text{otherwise.} \end{cases} \quad (3)$$

2.3 Heatfunction

One advantage of using a streamfunction in temperature–latitude space is that the MHT is easily computed via a cumulative integral in temperature (see e.g., Ferrari and Ferreira (2011)). This defines a *heatfunction*,

$$H(\phi, \theta, t) \stackrel{\text{def}}{=} \rho_0 c_p \int_{-2^\circ\text{C}}^{\theta} \Psi(\phi, \theta', t) d\theta', \quad (4)$$

where ρ_0 is reference density and c_p the specific heat capacity (both constants in our calculations since we use conservative temperature). The heatfunction (4) is equal to the cumulative MHT for waters colder than θ , and estimates the MHT of a closed circulation (in which mass is conserved) at a given latitude ϕ as:

$$\text{MHT}(\phi) = H(\phi, \theta^{\max}) - H(\phi, \theta^{\min}), \quad (5)$$

where θ^{\min} and θ^{\max} are the minimum and maximum temperatures spanned by the circulation cell. From (4) and (5), the MHT at a given latitude for each cell is directly proportional to its circulation strength and the temperature range spanned by that circulation (Ferrari & Ferreira, 2011).

The heatfunction for the flux-forced control simulation (Fig. 1f) is mostly positive and increases with temperature, demonstrating the dominant northward heat transport throughout the Atlantic associated with the clockwise circulation in the latitude–temperature plane. The total northward MHT, indicated by the value of the heatfunction at the maximum temperature, is largest in the subtropics.

3 Results

The MHT due to each cell, computed using (5), can vary between the simulations via: (*i*) adjustments in the circulation strength Ψ , (*ii*) modifications in the temperature range spanned by the circulation, or (*iii*) a combination of both of the above. These processes occur on different timescales, thus, we examine the MHT carried by each cell on short (1–10 years) and long (51–100 years) timescales.

3.1 Wind stress perturbation experiments

We analyze two perturbation experiments in which we change wind stress in the North Atlantic by a factor of 0.5 and 1.5 (labeled as $0.5 \times W$ and $1.5 \times W$ respectively) times the control (CTRL) value.

3.1.1 Initial response

The circulation strength at warm temperatures scales with the magnitude of wind stress on short timescales (compare streamfunction within red contour between Figs. 2a-c). These changes are primarily led by the warm cell, with a small contribution from the mixed cell (compare trends in the red and black text across experiments in Figs. 2a-c)). The circulation at cold temperatures weakens as the wind stress strengthens, which may be linked to increased southward near-surface Ekman transport in the subtropics and lesser waters being carried poleward to circulate within the cold cell.

In the first decade, changes in the circulation of each cell control the MHT anomalies, with little influence from changes in the temperature structure (compare temperature range in heatfunction plots between Figs. 2d-f). Thus, the warm cell's MHT scales with the magnitude of wind stress, whereas the cold cell's MHT is inversely related to the strength of wind stress. In contrast, the mixed cell does not show a clear signal in the first 10 years. These MHT anomalies gradually modify the ocean's near-surface meridional thermal structure (Figs. 2d-f). A reduction in the cold cell's MHT in the $1.5 \times W$ experiment contributes to cooler temperatures north of $35^\circ N$. In contrast, water is warmer in the $0.5 \times W$ experiment north of $35^\circ N$. Similarly, stronger northward heat transport by the warm cell in $1.5 \times W$ contributes to cooling the tropics, while weaker MHT in the $0.5 \times W$ leads to warmer tropics.

3.1.2 Long-term response

The circulation anomalies for warm and mixed cells do not change significantly compared to the first 10 years, suggesting a quick wind-driven adjustment. The cold cell is minutely affected by Atlantic-only wind stress variations on long timescales (compare Figs. 2g-i). Conversely, experiments with global wind stress perturbations (not shown) produce a direct scaling between the cold cell's circulation strength and the magnitude of wind stress, which is likely due to anomalous wind-driven upwelling in the Southern Ocean that plays a key role in modulating the cold cell (Cessi, 2019). Variations in the circulation-driven MHT thermally restructure each cell. For example, the temperature distribution anomalies observed in the tropics and high-latitudes in the first 10 years (Figs. 2a-c) are amplified in the last 50 years (Figs. 2g-i).

On long timescales, modifications in the ocean's temperature partially compensate for circulation-driven MHT changes (compare Figs. 2j-l) for the mixed cell. Variations in circulation dominate over temperature distribution anomalies, thus, the MHT carried by the mixed cell increases. On the other hand, anomalies in the circulation and temperature distribution act in concert for the warm and cold cells. Therefore, the warm cell carries more heat as the wind stress strengthens while the cold cell's MHT reduces as the wind stress intensifies. However, the total Atlantic MHT remains the same since the total surface heat fluxes are fixed across the three experiments. Such compensation in the MHT anomalies

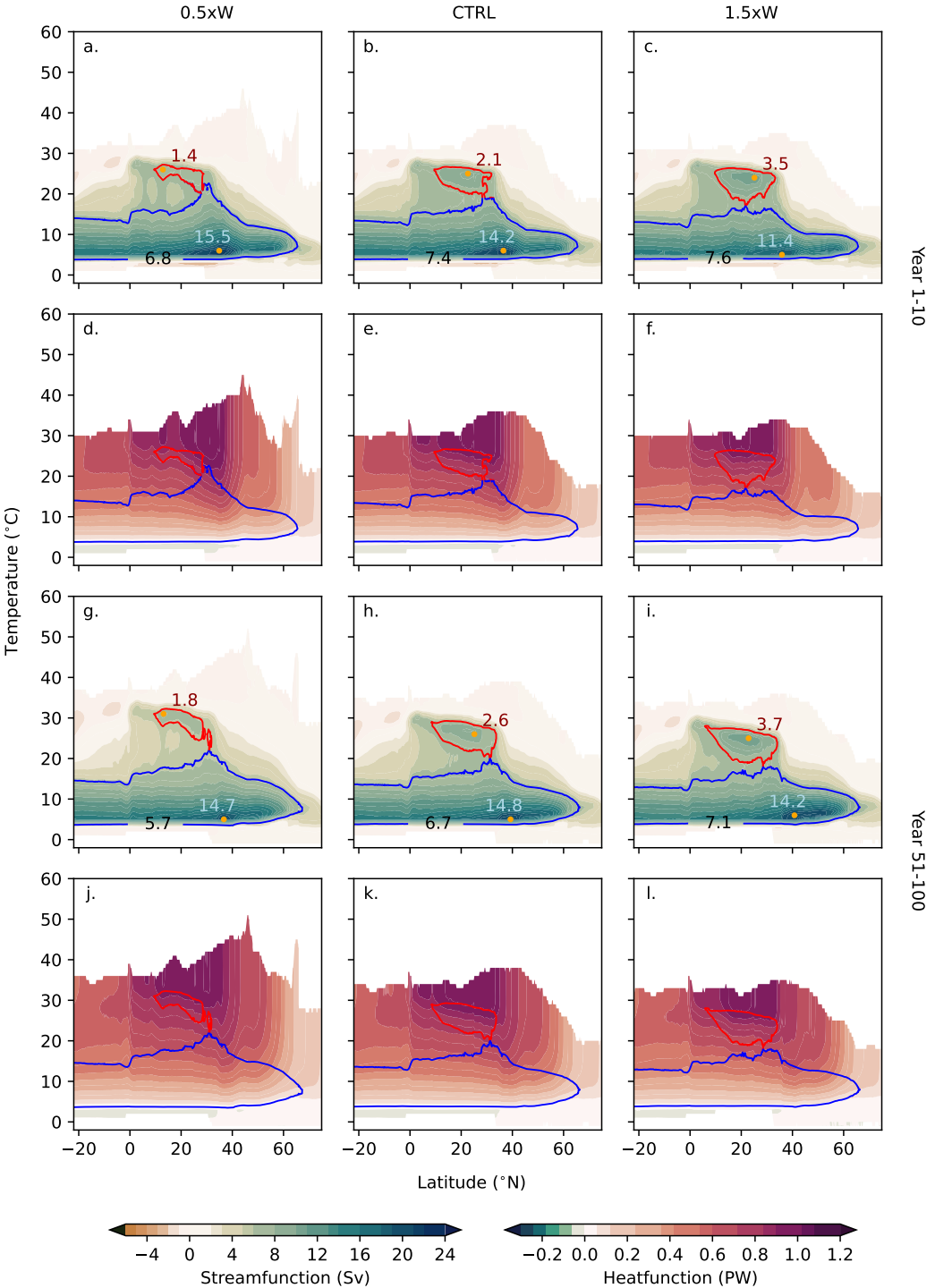


Figure 2. Rows 1/3: Streamfunction in latitude–temperature space (left colorbar) calculated from the first 10 (a-c) and last 50 years (g-i) for the $0.5 \times W$ (left), CTRL (middle), and $1.5 \times W$ (right) experiments. The strength of the mixed cell (black text), the warm cell (red text), and the cold cell (blue text) are indicated. Rows 2/4: Heatfunction in rows 1 and 3 for the first 10 (d-f) and last 50 years (j-l) for the $0.5 \times W$ (left), CTRL (middle), and $1.5 \times W$ (right) experiments.

between the three cells is not observed in the wind perturbation experiments by Ferrari and Ferreira (2011), since their surface buoyancy forcing varies with different values of wind stress. To summarize, the total MHT is unchanged in our experiments on long timescales, but the proportion of heat carried by the warm and mixed cells increases with wind stress at the expense of the cold cell.

3.2 Surface buoyancy flux contrast experiments

We now examine the response of each cell's circulation and heat transport to an increase and reduction in the North Atlantic surface meridional heat flux contrast, as quantified by -20 W m^{-2} and $+20 \text{ W m}^{-2}$ simulations. Since we apply anomalous surface meridional heat flux gradients, we expect variations in the total Atlantic MHT.

3.2.1 Initial response

In the first 10 years, the cold cell's circulation scales with the surface heat flux contrast (compare blue text between Figs. 3a-c). Subpolar surface cooling in the $+20 \text{ W m}^{-2}$ experiment enhances deep water formation and strengthens the cold cell, while subpolar heating in the -20 W m^{-2} experiment weakens its circulation. The warm and mixed cells weaken in the first 10 years as the surface meridional heat flux contrast increases (black text in Figs. 3a-c).

Similar to wind stress perturbations, modifications in the Atlantic MHT stem primarily from changes in the circulation in the first 10 years. Since the cold cell's circulation increases with the surface heat flux contrast, its heat transport also scales similarly (compare heatfunction plots between Figs. 3d-f). Conversely, the warm and mixed cells' MHT slightly reduce as the surface meridional heat flux contrast increases. In the first 10 years, the temperature distribution is largely affected by localized surface heat flux anomalies rather than by circulation-driven MHT variations. For example, anomalous surface heating raises the maximum temperature in subpolar regions in the -20 W m^{-2} experiment and in the subtropics in the $+20 \text{ W m}^{-2}$ experiment.

3.2.2 Long-term response

On long timescales, the temperature distribution within each cell is controlled by a combination of remote circulation-driven MHT variations and localized surface heat flux anomalies. We find modifications in each cell's temperature distribution across all latitudes (see Figs. 3g-i). For example, the maximum temperature reduces in the -20 W m^{-2} experiment and increases in the $+20 \text{ W m}^{-2}$ experiment even for latitudes south of 10°N where no anomalous surface heat flux is applied.

We find that variations in the warm and cold cells' strength and temperature distribution act jointly to influence the Atlantic MHT on long timescales (compare the heatfunction plots between Figs. 3j-l). The temperature ranges occupied by the two cells reduces in the -20 W m^{-2} experiment and increases in the $+20 \text{ W m}^{-2}$ experiment. Thus, the MHT carried by the two cells scale with the surface meridional heat flux contrast. It is interesting that the warm cell's circulation shows a trend reversal compared to the first 10 years. The long-term trend is consistent with recent studies (Hogg & Gayen, 2020; Bhagtani et al., 2023b) demonstrating that the near-surface circulation scales with the surface meridional heat flux contrast. In contrast to the warm and cold cells, variations in the temperature distribution and circulation strength compensate the mixed cell's MHT anomalies to a large extent. As the surface meridional heat flux contrast increases, the mixed cell weakens but occupies a larger temperature range. Variations in the circulation dominate over the temperature distribution anomalies; thus, the mixed cell's MHT reduces as the surface heat flux contrast increases. The MHT reduction in the mixed cells almost entirely negates the MHT increase by the warm and cold cells as we increase the surface meridional heat flux

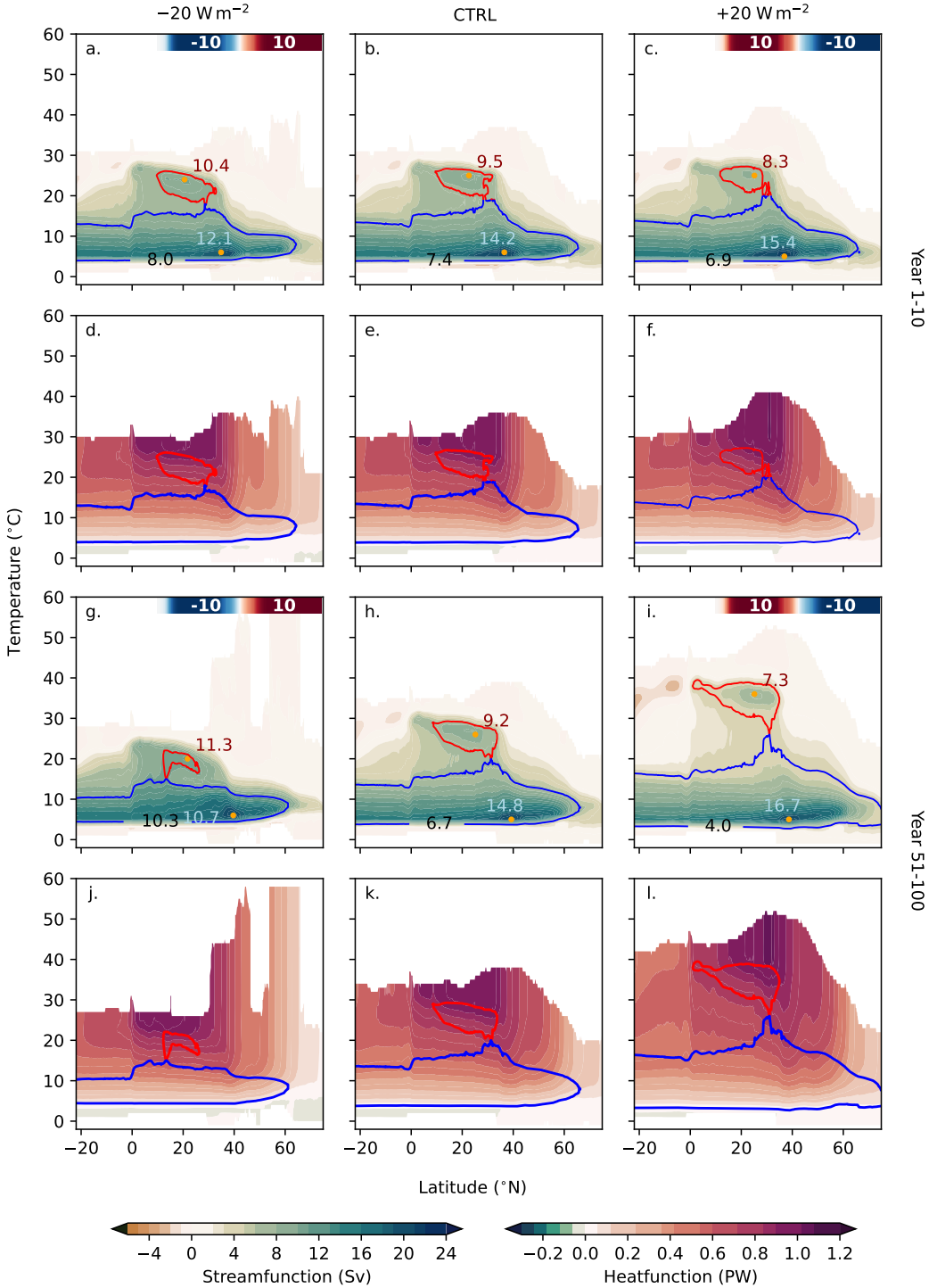


Figure 3. Rows 1/3: Streamfunction in latitude–temperature space from the first 10 (a-c) and last 50 years (g-l) for the -20 W m^{-2} (left column), CTRL (middle column), and $+20 \text{ W m}^{-2}$ (right column) experiments. The strength of the mixed cell (black text), the warm cell (red text), and the cold cell (blue text) are indicated. The colorbar at the top of (a), (c), (g), and (i) indicates the anomalous surface heat fluxes (in W m^{-2}). Rows 2/4: Heatfunction in rows 1 and 3 for the first 10 (d-f) and last 10 years (j-l) of the surface meridional heat flux contrast perturbation experiments.

gradients. Overall, as expected, the total Atlantic MHT scales with the surface meridional heat flux contrast (Figs. 3h-j).

4 Summary and discussion

In this study, we use a series of global ocean simulations to quantify the independent effects of wind stress and surface heat fluxes in steering the North Atlantic MHT. We divide the Atlantic circulation into warm (gyre), cold (meridional overturning), and mixed circulations in latitude–temperature space following Ferrari and Ferreira (2011) to understand the sensitivity of each circulation’s MHT to varying surface forcing.

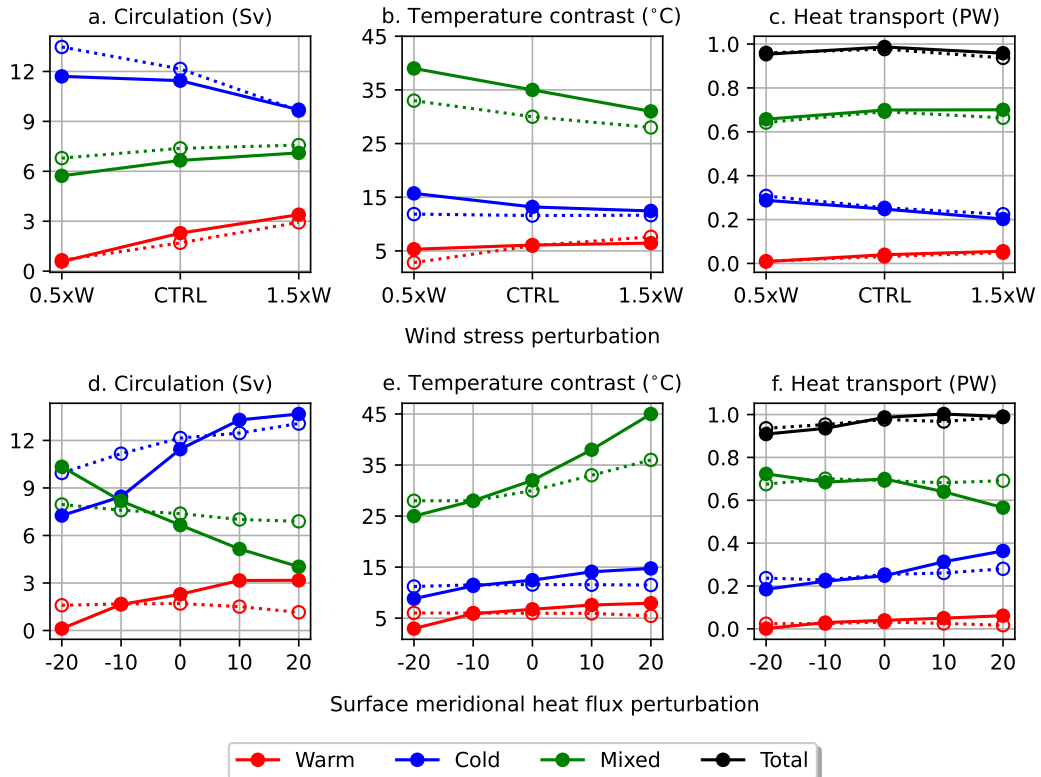


Figure 4. Metrics for meridional heat transport for the first 10 years (dashed lines) and last 50 years (solid lines) for the wind perturbation (top row) and surface meridional heat flux perturbation (bottom row) experiments.

We select the 26°N transect to summarize the changes in circulation, MHT, and the relative contributions of the three cells. Contrary to the literature, we find more interconnected roles of wind stress and surface buoyancy forcing in steering the MHT by the near-surface and deep circulations (Figs. 4c, f). The warm and mixed cell’s MHT increase with the wind stress. The total MHT in these wind stress perturbation experiments (in which we maintain the same surface buoyancy fluxes) should converge to the CTRL’s MHT as we progress towards equilibrium. We find that this is achieved through a reduction in the cold cell’s MHT that compensates the increased heat carried by the warm and mixed cells on long timescales.

The warm cell’s MHT scales not only with the wind stress, but also with the surface meridional heat flux contrast. However, in these surface meridional heat flux contrast per-

turbation experiments, the cold cell's MHT also increases, with significant compensation by a reduction in the heat transport associated with the mixed cell; thus, enhanced buoyancy forcing strengthens the distinction between warm and cold cells. We observe that the mixed cell's MHT is more sensitive to changes in surface heat fluxes than to wind stress variations on long timescales.

The MHT of the warm, cold, and mixed cells adjust to changes in winds and surface heat fluxes through three mechanisms: (*i*) changes in circulation strength, (*ii*) variations in the temperature distribution of each cell (i.e., the average temperature difference between the northward and southward flowing arms of the cell), or (*iii*) a combination of both. Anomalies in circulation dominate the MHT variations on short timescales. These MHT variations then affect the temperature ranges spanned by each circulation, which then feed back onto the MHT on long timescales through the temperature contrast between the two arms of each cell. Both the circulation- and temperature-driven MHT variations act jointly for the warm and cold cells due to independent variations in wind stress (Figs. 4a-b) and surface meridional heat flux gradients (Figs. 4d-e). It is worth mentioning that the warm cell's circulation scales with the surface meridional heat flux contrast on long timescales (red line in Fig. 4d), consistent with recent studies (Hogg & Gayen, 2020; Bhagtani et al., 2023b) demonstrating a role of surface buoyancy forcing in steering the gyre circulation. The temperature-driven MHT variations partially compensate circulation-driven MHT variations for the mixed cell (green line in Figs. 4d-e). Thus, our analysis underscores the distinct pathways utilized by the three cells to respond to varying surface forcing.

In reality, the wind stress and surface buoyancy forcing are strongly coupled and depend on the ocean response itself. In particular, the surface heat flux depends strongly on the ocean's sea surface temperature, which responds dynamically to heat transport changes associated with both winds and surface heat fluxes. In the absence of a restoring, the flux-forced simulations show a higher SST variance that is partly attributed to reduced damping of mesoscale eddies, but also partly caused by interannual-to-multidecadal variability in the North Atlantic. However, since the ocean's MHT is majorly driven by the time-mean MHT (Yung & Holmes, 2023), the higher SST variance does not affect our results to leading order.

Our flux-forced simulations, along with a decomposition of the Atlantic circulation into warm, cold, and mixed cells, provide useful insights into how the Atlantic Ocean's MHT may respond to climate change. For example, climate projections suggest a strengthening of zonal winds (Shaw & Miyawaki, 2024). Under such scenarios, our results indicate an increased contribution of the warm cell to northward heat transport, led by a spin up of the subtropical gyre. At the same time, projected melting in the Greenland and the Arctic (Rantanen et al., 2022) will likely reduce surface buoyancy loss in the North Atlantic leading to a reduction in the MHT carried by the AMOC. Under either scenario, the mixed circulation is expected to intensify, implying (*i*) a stronger coupling between near-surface and deep circulations, and (*ii*) a larger proportion of the Atlantic Ocean's MHT being carried by water masses that can transit between the subtropical gyre and the AMOC.

Open Research Section

Notebooks used for reproducing the analyses and figures are available at the repository github.com/dhruvbhagtani/Atlantic-meridional-heat-transport-heatfunction. Preprocessed data for the flux-forced simulations is available online at Bhagtani et al. (2023a). The modified MOM5 source code for the flux-forced simulations used in this paper is available at github.com/dhruvbhagtani/MOM5. Our analyses were facilitated with the Python packages `dask` (Rocklin, 2015) and `xarray` (Hoyer & Hamman, 2017).

Acknowledgments

We thank Christopher Bladwell, William Johns, Spencer Jones, and the Consortium for

Ocean–Sea Ice Modeling in Australia (cosima.org.au) for fruitful discussions and for maintaining the Cookbook of analysis recipes (Constantinou et al., 2024). We also thank the editor and three anonymous reviewers for their constructive comments. Computational resources were provided by the National Computational Infrastructure, which is supported by the Commonwealth Government of Australia. We acknowledge funding from the Australian National University under the University Research Scholarship (D.B.) and from the Australian Research Council under DECRA Fellowships DE210100004 (R.M.H.) and DE210100749 (N.C.C.).

References

- Abernathay, R. P., Gnanadesikan, A., Pradal, M.-A., & Sundermeyer, M. A. (2022). Chapter 9 - Isopycnal mixing. In M. Meredith & A. Naveira Garabato (Eds.), *Ocean mixing* (p. 215-256). Elsevier. doi: 10.1016/B978-0-12-821512-8.00016-5
- Berglund, S., Döös, K., Groeskamp, S., & McDougall, T. J. (2022). The downward spiralling nature of the North Atlantic subtropical gyre. *Nature Communications*, 13, 1-9. doi: 10.1038/s41467-022-29607-8
- Bhagtnani, D., Hogg, A. M., Holmes, R. M., & Constantinou, N. C. (2023a). Data related to the paper: Surface Heating Steers Planetary-Scale Ocean Circulation [Dataset]. *in Journal of Physical Oceanography*. Zenodo. doi: 10.5281/zenodo.8405009
- Bhagtnani, D., Hogg, A. M., Holmes, R. M., & Constantinou, N. C. (2023b). Surface heating steers planetary-scale ocean circulation. *Journal of Physical Oceanography*, 53, 2375–2391. doi: 10.1175/JPO-D-23-0016.1
- Boccaletti, G., Ferrari, R., Adcroft, A., Ferreira, D., & Marshall, J. (2005). The vertical structure of ocean heat transport. *Geophysical Research Letters*, 32. doi: 10.1029/2005GL022474
- Bryan, K. (1982). Seasonal variation in meridional overturning and poleward heat transport in the Atlantic and Pacific oceans: a model study. *Journal of Marine Research*, 40, 39-53.
- Bryan, K. (1991). Poleward heat transport in the ocean. *Tellus A*, 43, 104-115. doi: 10.1034/j.1600-0870.1991.00009.x
- Bryden, H., & Imawaki, S. (2001). Chapter 6.1 Ocean heat transport. In G. Siedler, J. Church, & J. Gould (Eds.), *Ocean circulation and climate* (Vol. 77, p. 455-474). Academic Press. doi: 10.1016/S0074-6142(01)80134-0
- Cessi, P. (2019). The global overturning circulation. *Annu. Rev. Mar. Sci*, 11, 249-270. doi: 10.1146/annurev-marine-010318
- Constantinou, N. C., Hogg, A. M., Gibson, A., Beucher, R., Heerdegen, A., Steketee, A., ... Zika, J. (2024). *COSIMA Cookbook: v0.1.0*. Zenodo. doi: 10.5281/zenodo.14353853
- Ferrari, R., & Ferreira, D. (2011). What processes drive the ocean heat transport? *Ocean Modelling*, 38, 171-186. doi: 10.1016/j.ocemod.2011.02.013
- Frajka-Williams, E., Ansorge, I. J., Baehr, J., Bryden, H. L., Chidichimo, M. P., Cunningham, S. A., ... Wilson, C. (2019). Atlantic Meridional Overturning Circulation: Observed transport and variability. *Frontiers in Marine Science*, 6. doi: 10.3389/fmars.2019.00260
- Greatbatch, R. J., & Zhai, X. (2007). The generalized heat function. *Geophysical Research Letters*, 34. doi: 10.1029/2007GL031427
- Griffies, S. M. (2012). *Elements of the Modular Ocean Model (MOM) 2012 release with updates*. Retrieved from www.gfdl.noaa.gov/fms.
- Hall, M. M., & Bryden, H. L. (1982). Direct estimates and mechanisms of ocean heat transport. *Deep Sea Research Part A, Oceanographic Research Papers*, 29, 339-359. doi: 10.1016/0198-0149(82)90099-1
- Hogg, A. M., & Gayen, B. (2020, 8). Ocean gyres driven by surface buoyancy forcing. *Geophysical Research Letters*, 47, 1-10. doi: 10.1029/2020GL088539
- Holmes, R. M., Zika, J. D., Ferrari, R., Thompson, A. F., Newsom, E. R., & England, M. H. (2019). Atlantic ocean heat transport enabled by indo-Pacific heat uptake and mixing.

- Geophysical Research Letters*, 46. doi: 10.1029/2019GL085160
- Hoyer, S., & Hamman, J. (2017). xarray: N-D labeled arrays and datasets in Python. *Journal of Open Research Software*, 5, 1-10. doi: 10.5334/jors.148
- Johns, W. E., Baringer, M. O., Beal, L. M., Cunningham, S. A., Kanzow, T., Bryden, H. L., ... Curry, R. (2011). Continuous, array-based estimates of Atlantic ocean heat transport at 26.5°N. *Journal of Climate*, 24, 2429-2449. doi: 10.1175/2010JCLI3997.1
- Johns, W. E., Eliot, S., Smeed, D. A., Moat, B., King, B., Volkov, D. L., & Smith, R. H. (2023). Towards two decades of Atlantic ocean mass and heat transports at 26.5°N. *Philosophical Transactions of the Royal Society A: Mathematical, Physical and Engineering Sciences*, 381, 20220188. doi: 10.1098/rsta.2022.0188
- Jones, S. C., Jiang, S., & Abernathey, R. P. (2024). A comparison of diagnostics for AMOC heat transport applied to the CESM large ensemble. *Journal of Advances in Modeling Earth Systems*, 16(8), e2023MS003978. doi: 10.1029/2023MS003978
- Kiss, A. E., Hogg, A. M., Hannah, N., Dias, F. B., Brassington, G. B., Chamberlain, M. A., ... Zhang, X. (2020, 2). ACCESS-OM2 v1.0: a global ocean–sea ice model at three resolutions. *Geoscientific Model Development*, 13, 401-442. doi: 10.5194/gmd-13-401-2020
- Liu, C., Yang, Y., Liao, X., Cao, N., Liu, J., Ou, N., ... Zheng, R. (2022). Discrepancies in simulated ocean net surface heat fluxes over the North Atlantic. *Advances in Atmospheric Sciences*, 39, 1941-1955. doi: 10.1007/s00376-022-1360-7
- Locarnini, R. A., Mishonov, A. V., Antonov, J. I., Boyer, T. P., Garcia, H. E., Baranova, O. K., ... Seidov, D. (2013). *World Ocean Atlas 2013. vol. 1: Temperature.* (Vol. 73).
- Masuda, K. (1988). Meridional heat transport by the atmosphere and the ocean: analysis of FGGE data. *Tellus, Series A*, 40 A, 285-302. doi: 10.3402/tellusa.v40i4.11801
- McDougall, T. J., & Barker, P. M. (2011). Getting started TEOS-10 and the Gibbs Seawater (GSW) oceanographic toolbox. *SCOR/IAPSO WG*, 127, 1–28.
- Mecking, J. V., & Drijfhout, S. S. (2023). The decrease in ocean heat transport in response to global warming. *Nature Climate Change*, 13, 1229-1236.
- Msadek, R., Johns, W. E., Yeager, S. G., Danabasoglu, G., Delworth, T. L., & Rosati, A. (2013). The Atlantic meridional heat transport at 26.5°N and its relationship with the MOC in the RAPID array and the GFDL and NCAR coupled models. *Journal of Climate*, 26, 4335-4356. doi: 10.1175/JCLI-D-12-00081.1
- Rantanen, M., Karpechko, A. Y., Lipponen, A., Nordling, K., Hyvärinen, O., Ruosteenoja, K., ... Laaksonen, A. (2022). The Arctic has warmed nearly four times faster than the globe since 1979. *Communications Earth & Environment*, 3, 168. doi: 10.1038/s43247-022-00498-3
- Rocklin, M. (2015). Dask: Parallel Computation with Blocked algorithms and Task Scheduling. In K. Huff & J. Bergstra (Eds.), (p. 130-136). Proceedings of the 14th Python in Science Conference. doi: 10.25080/Majora-7b98e3ed-013
- Shaw, T. A., & Miyawaki, O. (2024). Fast upper-level jet stream winds get faster under climate change. *Nature Climate Change*, 14, 61-67. doi: 10.1038/s41558-023-01884-1
- Stepanov, V. N., Iovino, D., Masina, S., Storto, A., & Cipollone, A. (2016). Methods of calculation of the Atlantic meridional heat and volume transports from ocean models at 26.5°N. *Journal of Geophysical Research: Oceans*, 121. doi: 10.1002/2015JC011007
- Sverdrup, H. U. (1947). Wind-driven currents in a baroclinic ocean; with application to the equatorial currents of the eastern Pacific. *Proceedings of the National Academy of Sciences*, 33, 318-326. doi: 10.1073/pnas.33.11.318
- Talley, L. D. (2003). Shallow, intermediate, and deep overturning components of the global heat budget. *Journal of Physical Oceanography*, 33, 530-560. doi: 10.1175/1520-0485(2003)033<0530:SIADOC>2.0.CO;2
- Trenberth, K. E., Zhang, Y., Fasullo, J. T., & Cheng, L. (2019). Observation-based estimates of global and basin ocean meridional heat transport time series. *Journal of Climate*, 32, 4567-4583. doi: 10.1175/JCLI-D-18-0872.1
- Tsujino, H., Urakawa, S., Nakano, H., Small, R. J., Kim, W. M., Yeager, S. G., ... Ya-

- mazaki, D. (2018, 10). JRA55 based surface dataset for driving ocean–sea-ice models (JRA55-do). *Ocean Modelling*, 130, 79-139. doi: 10.1016/j.ocemod.2018.07.002
- Wunsch, C., & Roemmich, D. (1985). Is the North Atlantic in Sverdrup balance? *Journal of Physical Oceanography*, 15. doi: 10.1175/1520-0485(1985)015<1876:itnais>2.0.co;2
- Xu, X., Rhines, P. B., & Chassignet, E. P. (2016). Temperature-salinity structure of the North Atlantic circulation and associated heat and freshwater transports. *Journal of Climate*, 29, 7723-7742. doi: 10.1175/JCLI-D-15-0798.1
- Yung, C. K., & Holmes, R. M. (2023). On the contribution of transient diabatic processes to ocean heat transport and temperature variability. *Journal of Physical Oceanography*. doi: 10.1175/JPO-D-23-0046.1
- Zweng, M. M., Reagan, J., Antonov, J., Mishonov, A., Boyer, T., Garcia, H., ... Bidle, M. (2013). *World Ocean Atlas 2013, volume 2: Salinity* (Vol. 2).